Time-Optimal Anti-Sloshing Trajectory Planning for Multiple Liquid-Filled Containers Subject to SCARA Motion

Andrea Ferrari, *Graduate Student Member, IEEE*, Roberto Di Leva, Simone Soprani, Luigi Biagiotti, *Member, IEEE*, Gianluca Palli, *Senior Member, IEEE*, and Marco Carricato, *Senior Member, IEEE*

***Abstract*—This paper develops algorithms for planning time-optimal pick-and-place trajectories for multiple cylindrical containers filled with liquid and simultaneously transported by a robot. The considered trajectories comprise 3D translations combined with a 1D rotation about the vertical direction, i.e. SCARA motions. The presented approach minimizes the execution time, while ensuring that the liquid surface within each container remains below an imposed threshold throughout the motion. Two types of optimal trajectories are studied: one optimizes the motion law along a given path, the other optimizes both the path and the motion law. Extensive simulations identify the most efficient optimization setup, whereas experiments validate the approach. The data sets of all simulated and experimental motions are distributed through an external repository.**

***Index Terms*—Motion and path planning, industrial robots, optimization and optimal control, sloshing dynamics.**

I. Introduction

MANY industrial processes involve the transportation of containers partially filled with liquid, such as bottles, vials, etc. The liquid oscillation inside the container, known as *sloshing*, can cause problems such as spillage, inconsistent fill levels, solid deposit on the vessel walls, etc. This paper investigates anti-sloshing trajectories for the simultaneous transport of multiple cylindrical containers. The trajectory duration must be as short as possible, while the peak reached by the liquid in each container, referred as *maximum sloshing height*, must remain under a specified threshold. The considered trajectories are 4D SCARA motions, comprising 3D translation combined with 1D rotation about the vertical direction, commonly found in many pick-and-place operations in pharmaceutical and food-and-beverage automated lines. All containers are mounted on a tray attached to the end-effector (EE) of a robot, so that each container undergoes different dynamics depending on its distance from the instantaneous rotation axis.

The literature offers several approaches for sloshing reduction. Filters represent a widely used technique to eliminate specific frequency components and reduce vibrations, including finite (FIR) and infinite (IIR) impulse response filters and exponential filters [1], [2]; a specific class of FIR filters, known as input shaping [3], is especially popular. A comparison of several filtering techniques for sloshing mitigation is available in [4]. Although filters are widely used to mitigate residual oscillations at the end of motion, they have several limitations that make them unsuitable for the case at hand: (i) they cannot constrain the maximum sloshing height during movement; (ii) there is no state-of-the-art way to apply them when the containers on the tray have distinct dynamics; (iii) they operate on preset motion laws and add delays, providing no direct means to achieve time-optimal trajectories. Tilting compensation is another common sloshing-suppression technique [5], but it cannot be used in the case under consideration, where only rotations about the vertical direction are allowed.

An alternative approach involves constrained optimization, where the goal is to minimize the trajectory duration while ensuring that the sloshing heights in all containers remain below a specified threshold throughout the robot motion. In [6], [7], this technique is applied to a single container subjected to 3D translational motion, but sloshing is mitigated by tilting the EE about horizontal axes. In [8], the segment durations of a piecewise motion law are optimized, but only 1D translation of a single container is considered. In [9], constrained optimization is used for generating a 4D SCARA trajectory of a single container, but sloshing mitigation is separately handled using shaping techniques. Constrained optimization is also employed in [10], [11] to plan anti-sloshing trajectories along predefined paths, and in [12] to design point-to-point motions. These optimizations are solved using a multiple shooting method implemented with CasADi [13], a software framework for nonlinear optimization in MATLAB. However, [10] and [11] only deal with 2D translations of a single container, whereas [12] does not constrain the maximum sloshing height within the optimizer, but it determines, using experimental methods and CFD techniques (both of which are time-consuming and not easy

Received 26 July 2025; accepted 19 November 2025. Date of publication 11 December 2025; date of current version 23 December 2025. This work was supported by FISA2023 Project *APACHE* under Grant CUP J53C25000520001 and in part by PRIN2020 Project *Co-Mir* under Grant 2020CMEFPK. This article was recommended for publication by Associate Editor A. Swikir and Editor L. Pallottino upon evaluation of the reviewers' comments. *(Corresponding author: Marco Carricato.)*

Andrea Ferrari, Roberto Di Leva, and Marco Carricato are with the Department of Industrial Engineering, University of Bologna, 40131 Bologna, Italy (e-mail: andrea.ferrari52@unibo.it; roberto.dileva@unibo.it; marco.carricato@unibo.it).

Simone Soprani and Gianluca Palli are with the Department of Electrical, Electronic and Information Engineering, University of Bologna, 40131 Bologna, Italy (e-mail: simone.soprani2@unibo.it; gianluca.palli@unibo.it).

Luigi Biagiotti is with the Department of Engineering, University of Modena and Reggio-Emilia, 41100 Modena, Italy (e-mail: luigi.biagiotti@unimore.it).

Digital Object Identifier 10.1109/LRA.2025.3643281

TABLE I
COMPARISON WITH STATE-OF-THE-ART CONTRIBUTIONS (IN PREHENSILE MANIPULATION, THE CONTAINERS ARE FIRMLY ATTACHED TO THE TRAY, WHEREAS IN THE NON-PREHENSILE CASE, THEY ARE SIMPLY PLACED ON IT)

Reference	Allowed motions				Number of containers	Manipulation		Anti-sloshing	Approach	Experimental validation
	x	y	z	θ		Prehensile	Non-prehensile			
[10]	✓	✓			1	✓		✓	Constrained Optimization	✓
[11]	✓	✓			1		✓	✓	Constrained Optimization	
[12]	✓	✓	✓	✓	2		✓		Constrained Optimization + CFD	✓
[16]	✓				1	✓		✓	Filters	✓
[17]	✓	✓	✓		1	✓			Sloshing modeling	✓
This paper	✓	✓	✓	✓	arbitrary	✓		✓	Constrained Optimization	✓

to implement), the maximum liquid volume that can be safely contained without spillage during the trajectory. A constrained optimization technique similar to that used in [10], [11], [12] is adopted in this work, with the aim of extending this approach to *4D SCARA trajectories* of *multiple containers*, an aspect that, to the best of our knowledge, has not been previously addressed in the literature.

Since sloshing constraints must be incorporated into the optimization process, a reliable and computationally efficient model is required. An equivalent discrete mechanical model provides an optimal balance between accuracy and efficiency. The literature considers two main discrete approaches for modeling the sloshing dynamics inside a container [14]: the pendulum model [6], [7], [9] and the mass-spring-damper (MSD) model [10], [15]. In particular, the latter model enables highly efficient estimation of sloshing height, based on a formulation proposed in [16] for 1D translational motions and extended in [17] to 3D translations. However, applications involving 4D motions have not yet been explored.

The original contributions of this paper are:

- the extension of the sloshing model in [16], [17] to 4D SCARA motions, involving 3D translations combined with a 1D rotation about the vertical direction;
- the identification of anti-sloshing trajectories for multiple containers, with distinct dynamics and possibly different geometries, handled simultaneously by the same robot;
- the comparison of two time-optimal trajectory-planning approaches, with one optimizing the motion law on an assigned path and the other optimizing both the path and the motion law;
- the experimental validation of the proposed approaches.

To better frame the contribution of the paper with respect to the existing literature, a comparison is presented in Table I .

The container geometry critically affects liquid behavior, influencing both model formulation and applicability. This work focuses on cylindrical containers, and examines geometries with different liquid height-to-radius ratios. Water is selected as the working fluid because its low viscosity enhances sloshing, making the problem more challenging.

The paper is structured as follows. Section II introduces the sloshing model. Section III presents the optimization algorithms. Section IV reports the experimental validation. Section V draws conclusions.

II. SLOSHING MODEL FOR 4D SCARA MOTION

A. Model Parameters

A cylindrical container with radius R is filled with a liquid of mass m_F. Under static conditions, the liquid height is h. The MSD model considers a mass m_0 fixed to the container and a series of sloshing masses m_n moving relative to the container (Fig. 1). Each mass is connected to a spring-damper system and its motion is described by the generalized coordinates (x_n, y_n, z_n), measured from the center-of-mass position of the undisturbed liquid, where frame $Oxyz$ is attached. The spring stiffness and the damping coefficient are k_n and c_n, respectively. The literature provides the model-parameter formulations by imposing equivalence between the discrete and the continuous model [14]. In particular, the natural frequency and the modal mass of the n-th mode are:

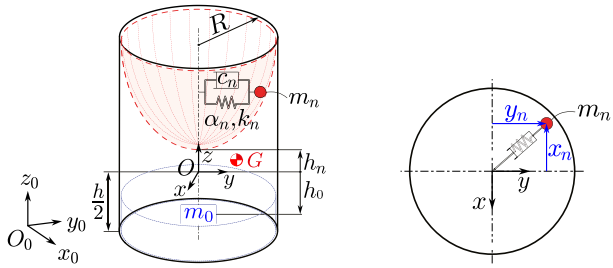

(a) Model Parameters. (b) Top view.

Fig. 1. MSD model.

$$\omega_n = \sqrt{\frac{k_n}{m_n}} = \sqrt{g\frac{\xi_{1n}}{R}\tanh\left(\xi_{1n}\frac{h}{R}\right)}, \tag{1}$$

$$m_n = m_F \frac{2R}{\xi_{1n}h(\xi_{1n}^2-1)}\tanh\left(\xi_{1n}\frac{h}{R}\right). \tag{2}$$

In (1) and (2), ξ_{1n} is the root of the derivative of the Bessel function of the first kind [18], and g is the gravitational acceleration. The damping ratio $\zeta_n = \dfrac{c_n}{2\sqrt{k_n m_n}}$ can be estimated by the experimental formula reported in [14]:

$$\zeta_n = 0.92\sqrt{\frac{\upsilon/\mu}{\sqrt{gR^3}}}\left[1+\frac{0.318}{\sinh(\xi_{1n}h/R)}\left(1+\frac{1-h/R}{\cosh(\xi_{1n}h/R)}\right)\right], \tag{3}$$

where υ and μ are the dynamic viscosity and density of the liquid, respectively.

The model in Fig. 1(a) considers the sloshing mass m_n as sliding on a paraboloidal surface [15], hence allowing the z-coordinate of m_n to be expressed in terms of (x_n, y_n) as:

$$z_n = h_n + \frac{P_n}{2}(x_n^2 + y_n^2), \tag{4}$$

where

$$h_n = \frac{1}{2}h\left[1 - \frac{2R\tanh\left(\xi_{1n}\frac{h}{R}\right)}{\xi_{1n}h}\right], \quad P_n = \frac{\omega_n^2}{g}. \tag{5}$$

Ref. [15] proposes to restrain the sloshing mass using a nonlinear spring of order w. This spring exerts the force

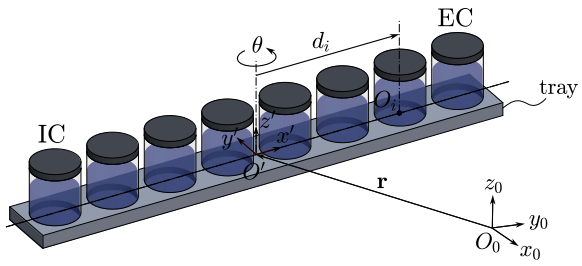

Fig. 2. Multi-container configuration.

$(\alpha/R^{2w-2})k_n\rho_n^{2w-1}$, where $\rho_n=\sqrt{x_n^2+y_n^2}$ is the radial coordinate of m_n, and parameters w and α are suggested in [15] to be set as $w=2$ and $\alpha\in[1/2,\ 2/3]$. However, an extensive experimental campaign recently conducted by the authors of this paper showed that a more conservative estimation of the sloshing height can be obtained by setting $\alpha=0$, namely removing the spring and only constraining m_n to move on the paraboloidal surface [19]. For this reason, we choose $\alpha=0$.

B. Equations of Motion and Sloshing Height Estimation

Given N_C containers mounted on a rigid support, $O_0x_0y_0z_0$ is a fixed reference frame, whereas $O'x'y'z'$ is a frame attached to the support. The containers may have different radii R_i and liquid static heights h_i. Since SCARA motions keep the container axes vertical, z' is always parallel to z_0, and θ can be defined as the angle between x' and x_0. Fig. 2 shows this configuration, in the case of 8 containers in a row.

If $\mathbf{r}$ is the position of O' in $O_0x_0y_0z_0$, the position of the center O_i of the base circle of the i-th container in $O_0x_0y_0z_0$ is:

$$\mathbf{r}_i=\mathbf{r}+\mathbf{R}_z(\theta)\mathbf{d}_i'=\mathbf{r}+\mathbf{d}_i, \tag{6}$$

where $\mathbf{d}_i'$ is the position vector from O' to O_i in $O'x'y'z'$, and $\mathbf{R}_z(\theta)$ is the rotation matrix about the z_0-axis by an angle θ. Differentiating (6) with respect to time gives the velocity and acceleration of the i-th container as:

$$\dot{\mathbf{r}}_i=\dot{\mathbf{r}}+\boldsymbol{\omega}\times\mathbf{d}_i,\quad \ddot{\mathbf{r}}_i=\ddot{\mathbf{r}}+\dot{\boldsymbol{\omega}}\times\mathbf{d}_i+\boldsymbol{\omega}\times(\boldsymbol{\omega}\times\mathbf{d}_i), \tag{7}$$

where $\boldsymbol{\omega}$ and $\dot{\boldsymbol{\omega}}$ are, respectively, the angular velocity and the angular acceleration of the tray.

The position vector $\mathbf{s}_{i,n}$ of the n-th sloshing mass in the generic container with respect to the fixed frame is:

$$\begin{aligned}\mathbf{s}_{i,n}&=\mathbf{r}_i+\mathbf{R}_z(\theta)\begin{bmatrix}x_{i,n}\\ y_{i,n}\\ \frac{h_i}{2}+z_{i,n}\end{bmatrix}\\ &=\begin{bmatrix}r_{i,x}+x_{i,n}\cos\theta-y_{i,n}\sin\theta\\ r_{i,y}+x_{i,n}\sin\theta+y_{i,n}\cos\theta\\ r_{i,z}+\frac{h_i}{2}+h_{i,n}+\dfrac{P_{i,n}}{2}(x_{i,n}^2+y_{i,n}^2)\end{bmatrix},\end{aligned} \tag{8}$$

where the subscript i added to the quantities defined in (1) through (4) identifies the i-th container.

For assigned linear and angular accelerations $\ddot{\mathbf{r}}_i=[\ddot{r}_{i,x}\ \ddot{r}_{i,y}\ \ddot{r}_{i,z}]^T$ and $\dot{\boldsymbol{\omega}}=[0\ \ 0\ \ \ddot{\theta}]^T$ of the i-th container, the *equations of motion* (EOMs) of the n-th sloshing mass can be obtained from Lagrange equations:

$$\frac{d}{dt}\left(\frac{\partial T_{i,n}}{\partial\dot{q}}\right)-\frac{\partial T_{i,n}}{\partial q}+\frac{\partial V_{i,n}}{\partial q}+\frac{\partial D_{i,n}}{\partial\dot{q}}=0,\qquad q=x_{i,n},y_{i,n} \tag{9}$$

where $T_{i,n}$, $D_{i,n}$ and $V_{i,n}$ are, respectively, the kinetic energy, the Rayleigh dissipation function (that accounts for the energy dissipation due to the relative velocity of $m_{i,n}$ with respect to the container) and the potential energy:

$$\begin{aligned}&T_{i,n}=\frac{m_{i,n}}{2}\|\dot{\mathbf{s}}_{i,n}\|^2,\ D_{i,n}=\frac{c_{i,n}}{2}\left(\dot{x}_{i,n}^2+\dot{y}_{i,n}^2+\dot{z}_{i,n}^2\right),\\ &V_{i,n}=m_{i,n}gs_{i,n,z}.\end{aligned} \tag{10}$$

Substituting (10) in (9) yields the EOMs:

$$\begin{bmatrix}1+P_{i,n}^2x_{i,n}^2 & P_{i,n}^2x_{i,n}y_{i,n}\\ P_{i,n}^2x_{i,n}y_{i,n} & 1+P_{i,n}^2y_{i,n}^2\end{bmatrix}\begin{bmatrix}\ddot{x}_{i,n}\\ \ddot{y}_{i,n}\end{bmatrix}=\begin{bmatrix}a_{i,n}\\ b_{i,n}\end{bmatrix} \tag{11}$$

where:

$$\begin{aligned}a_{i,n}&=-P_{i,n}^2(\dot{x}_{i,n}^2+\dot{y}_{i,n}^2)x_{i,n}+(2\dot{\theta}\dot{y}_{i,n}+\dot{\theta}^2x_{i,n}+\ddot{\theta}y_{i,n})\\ &-\omega_{i,n}^2x_{i,n}-2\omega_{i,n}\zeta_{i,n}\left[\dot{x}_{i,n}+P_{i,n}^2(x_{i,n}\dot{x}_{i,n}+y_{i,n}\dot{y}_{i,n})x_{i,n}\right]\\ &-\ddot{r}_{i,x}\cos(\theta)-\ddot{r}_{i,y}\sin(\theta)-\ddot{r}_{i,z}P_{i,n}x_{i,n},\\ b_{i,n}&=-P_{i,n}^2(\dot{x}_{i,n}^2+\dot{y}_{i,n}^2)y_{i,n}+(-2\dot{\theta}\dot{x}_{i,n}+\dot{\theta}^2y_{i,n}-\ddot{\theta}x_{i,n})\\ &-\omega_{i,n}^2y_{i,n}-2\omega_{i,n}\zeta_{i,n}\left[\dot{y}_{i,n}+P_{i,n}^2(x_{i,n}\dot{x}_{i,n}+y_{i,n}\dot{y}_{i,n})y_{i,n}\right]\\ &+\ddot{r}_{i,x}\sin(\theta)-\ddot{r}_{i,y}\cos(\theta)-\ddot{r}_{i,z}P_{i,n}y_{i,n}.\end{aligned} \tag{12}$$

Numerical integration of (11) yields the generalized coordinates $(x_{i,n},y_{i,n})$. From the latter, the maximum sloshing height $\overline{\eta}_i$ at the container wall can be computed as shown in [16], [17]. If only the first mode is considered, as higher-order modes have a negligible impact on the sloshing behavior [14], [16], $\overline{\eta}_i$ can be computed as:

$$\overline{\eta}_i\approx\frac{\xi_{i,11}^2h_im_{i,1}}{m_{i,F}R_i}\sqrt{x_{i,1}^2+y_{i,1}^2}. \tag{13}$$

The subscript 1, referring to the first sloshing mode, is henceforth omitted.

III. Time-Optimal Trajectory Planning

The implementation details of the optimizations reported in Sections III-A and III-B can be found in Section IV-D.

A. Trajectories With an Assigned Path

In this case, the path that the tray (and hence the containers) must follow is predefined. Therefore, the optimization objective is to determine the motion law that allows the trajectory execution in minimal time, while at the same time binding the sloshing height under a specified threshold in all containers.

The path is parameterized in terms of a parameter $s\in[0,1]$, whose motion law $s(t)$, $\dot{s}(t)$, $\ddot{s}(t)$ describes the temporal evolution along the path. The position vector $\mathbf{r}$ and its time derivatives can be written as:

$$\mathbf{r}=\mathbf{r}(s),\quad \dot{\mathbf{r}}(s,\dot{s})=\mathbf{r}'(s)\dot{s},\quad \ddot{\mathbf{r}}(s,\dot{s},\ddot{s})=\mathbf{r}''(s)\dot{s}^2+\mathbf{r}'(s)\ddot{s}, \tag{14}$$

where $(\cdot)'$ denotes the derivative with respect to s. The relation between $\mathbf{r}$ and s is defined using B-spline functions:

$$\mathbf{r}(s)=\sum_{j=0}^{m}B_j^d(s)\mathbf{p}_j,\qquad s\in[0,1], \tag{15}$$

where $B_j^d(s)$ is the B-spline basis function of degree d (in our case $d=4$) and $\mathbf{p}_j$ is the generic control point.

While the jerks of s and θ could be used as control inputs to ensure a smooth trajectory ($\mathbf{u}=[\dddot{s},\dddot{\theta}]$), numerical investigation

showed that it is more efficient to use only the jerk of s as control input:

$$u = \dddot{s}, \tag{16}$$

and defining θ as a linear function of s, i.e.:

$$\theta = \theta_{start} + s \cdot (\theta_{end} - \theta_{start}), \qquad s \in [0,1], \tag{17}$$

where θ_{start} and θ_{end} denote the values of θ at the beginning and at the end of the trajectory. This choice reduces algorithm complexity and computation time, with only a marginal increase in trajectory duration.

The system state is defined by the following vector $\mathbf{x}$:

$$\mathbf{x} = [s \;\; \dot{s} \;\; \ddot{s} \;\; x_1 \;\; y_1 \;\; \dot{x}_1 \;\; \dot{y}_1 \;\; \ldots \;\; x_{N_C} \;\; y_{N_C} \;\; \dot{x}_{N_C} \;\; \dot{y}_{N_C}]^T, \tag{18}$$

which includes the path parameter and its time derivatives, as well as the variables (x_i, y_i), with $i = 1, \ldots, N_C$, and their time derivatives, identifying the motion of the first sloshing mass inside i-th container (Fig. 2).

Finally, if t_{end} is the trajectory duration, the optimization problem can be formulated as:

$$\min_{t_{end},\, u} \int_0^{t_{end}} \left[1 + k u(t)^2\right] dt \tag{19a}$$

subject to

$$\dot{\mathbf{x}}(t) = \mathbf{f}(\mathbf{x}(t), u(t)) \tag{19b}$$

$$\mathbf{x}(0) = [0 \;\; 0 \;\; 0 \;\; 0 \;\; 0 \;\; 0 \;\; 0 \;\; \ldots \;\; 0 \;\; 0 \;\; 0 \;\; 0]^T \tag{19c}$$

$$\mathbf{x}(t_{end}) = [1 \;\; 0 \;\; 0 \;\; 0 \;\; 0 \;\; - \;\; - \;\; \ldots \;\; 0 \;\; 0 \;\; - \;\; -]^T \tag{19d}$$

$$\overline{\eta}_i(t) \le \overline{\eta}_{lim}, \qquad i = 1, \ldots, N_C; \;\; t \in [0, t_{end}] \tag{19e}$$

$$\overline{\eta}_i(t) \le 0.2\overline{\eta}_{lim}, \qquad i = 1, \ldots, N_C; \;\; t > t_{end} \tag{19f}$$

$$|u(t)| \le u_{max}, \qquad t \in [0, t_{end}] \tag{19g}$$

$$|\dot{q}_j(t)| \le \dot{q}_{j,max}, \qquad j = 1, \ldots, 6; \;\; t \in [0, t_{end}]. \tag{19h}$$

The cost functional in (19a) is a trade-off between minimal time and minimal jerk of s, with weighting factor k. The function $\mathbf{f}$ in (19b) includes the integration chain of s from u and the sloshing dynamics of each container as obtained from (11), namely:

$$\frac{d}{dt}\begin{bmatrix} s & \dot{s} & \ddot{s} \end{bmatrix}^T = \begin{bmatrix} \dot{s} & \ddot{s} & u \end{bmatrix}^T \tag{20a}$$

$$\frac{d}{dt}\begin{bmatrix} x_i \\ y_i \end{bmatrix} = \begin{bmatrix} \dot{x}_i \\ \dot{y}_i \end{bmatrix}, \quad i = 1, \ldots, N_C \tag{20b}$$

$$\frac{d}{dt}\begin{bmatrix} \dot{x}_i \\ \dot{y}_i \end{bmatrix} = \begin{bmatrix} 1 + P_i^2 x_i^2 & P_i^2 x_i y_i \\ P_i^2 x_i y_i & 1 + P_i^2 y_i^2 \end{bmatrix}^{-1} \begin{bmatrix} a_i \\ b_i \end{bmatrix}, \quad i = 1, \ldots, N_C. \tag{20c}$$

The constraints in (19c, 19d) define the initial and final states of $\mathbf{x}$. The symbol "$-$" appearing in (19d) indicates that no final condition has been imposed on variables $\dot{x}_1(t_{end})$, $\dot{y}_1(t_{end})$, $\ldots$, $\dot{x}_{N_C}(t_{end})$ and $\dot{y}_{N_C}(t_{end})$. The constraint ensuring that the maximum sloshing heights remain below the threshold $\overline{\eta}_{lim}$ during motion is represented in (19e), while (19f) limits the residual liquid oscillations after the motion ends. Condition (19g) constrains the maximum absolute value of u: without this constraint, the optimizer may generate trajectories with excessively high jerk, which can compromise motion smoothness and feasibility. Condition (19h) ensures that joint velocities $\dot{q}_j$ remain within the robot physical limits. $\dot{\mathbf{q}}$ is computed from the EE twist through the Jacobian matrix $\mathbf{J}(\mathbf{q})$. The EE path is assumed to lie in the robot workspace and be nonsingular, so that $\mathbf{J}$ is a 6×6 invertible matrix. However, to enhance robustness in case of ill-conditioning of $\mathbf{J}$, a damped least-square pseudoinverse was used with a regularization factor of $\beta = 0.03$, namely $\mathbf{J}^\dagger = (\mathbf{J}^T\mathbf{J} + \beta^2\mathbf{I}_{6x6})^{-1}\mathbf{J}^T$, so that $\dot{\mathbf{q}} = \mathbf{J}^\dagger(\mathbf{q})[\dot{\mathbf{r}}^T, \boldsymbol{\omega}^T]^T$.

B. Point-to-Point Trajectories

This subsection investigates time-optimal trajectory planning along paths that are not completely assigned *a priori*. Only some way-volumes, through which optimal paths must pass, are assigned to the optimizer. Unlike the algorithm presented in Section III-A, a path parameter s cannot be used and the system state $\mathbf{x}$ must directly include the position vector $\mathbf{r} \in \mathbb{R}^3$ and the angle θ. Thus the control input is defined as:

$$\mathbf{u} = \begin{bmatrix} \mathbf{u}_r \\ u_\theta \end{bmatrix} = \begin{bmatrix} \dddot{\mathbf{r}} \\ \dddot{\theta} \end{bmatrix} = \begin{bmatrix} \dddot{r}_x & \dddot{r}_y & \dddot{r}_z & \dddot{\theta} \end{bmatrix}^T, \tag{21}$$

and the optimizer must provide the optimal trends for both $\mathbf{r}(t)$ and $\theta(t)$.

The system state is represented by the array $\mathbf{x}$:

$$\mathbf{x} = [\mathbf{r}^T \;\; \dot{\mathbf{r}}^T \;\; \ddot{\mathbf{r}}^T \;\; \theta \;\; \dot{\theta} \;\; \ddot{\theta} \;\; x_1 \;\; y_1 \;\; \dot{x}_1 \;\; \dot{y}_1 \;\; \ldots \;\; x_{N_C} \;\; y_{N_C} \;\; \dot{x}_{N_C} \;\; \dot{y}_{N_C}]^T. \tag{22}$$

The optimization problem is formulated as:

$$\min_{t_{end},\, \mathbf{u}} \int_0^{t_{end}} \left[1 + k_r \mathbf{u}_r(t)^T \mathbf{u}_r(t) + k_\theta u_\theta(t)^2\right] dt \tag{23a}$$

subject to

$$\dot{\mathbf{x}}(t) = \mathbf{f}(\mathbf{x}(t), \mathbf{u}(t)) \tag{23b}$$

$$\mathbf{x}(0) = [\; \mathbf{r}_0^T \;\; \mathbf{0}^T \;\; \mathbf{0}^T \;\; \theta_{start} \; 0 \; 0 \; 0 \; 0 \; 0 \;\; \ldots \; 0 \; 0 \; 0 \; 0 \;]^T \tag{23c}$$

$$\mathbf{x}(t_{end}) = [\mathbf{r}_{end}^T \;\; \mathbf{0}^T \;\; \mathbf{0}^T \;\; \theta_{end} \;\; 0 \; 0 \; 0 \; 0 - - \ldots \; 0 \; 0 - -]^T \tag{23d}$$

$$\overline{\eta}_i(t) \le \overline{\eta}_{lim} \qquad i = 1, \ldots, N_C; \;\; t \in [0, t_{end}] \tag{23e}$$

$$\overline{\eta}_i(t) \le 0.2\overline{\eta}_{lim} \qquad i = 1, \ldots, N_C; \;\; t > t_{end} \tag{23f}$$

$$|\mathbf{u}_r(t)| \le \mathbf{u}_{r,max}; |u_\theta(t)| \le u_{\theta,max} \qquad t \in [0, t_{end}] \tag{23g}$$

$$\delta^2 \ge (\mathbf{r}(t_j) - \mathbf{r}_j)^T (\mathbf{r}(t_j) - \mathbf{r}_j) \qquad j = 1, \ldots, n_v \tag{23h}$$

$$\mathbf{r}_{min} \le \mathbf{r}(t) \le \mathbf{r}_{max} \qquad t \in [0, t_{end}] \tag{23i}$$

$$q_{j,min} \le q_j(t) \le q_{j,max} \quad j = 1, \ldots, 6; \;\; t \in [0, t_{end}] \tag{23j}$$

$$|\dot{q}_j(t)| \le \dot{q}_{j,max} \qquad j = 1, \ldots, 6; t \in [0, t_{end}] \tag{23k}$$

$$[\kappa(\mathbf{J})]^{-1} \ge k_{cond} \qquad t \in [0, t_{end}]. \tag{23l}$$

The tuning factors k_r and k_θ in (23a) weigh the jerks of $\mathbf{r}$ and θ. The function $\mathbf{f}$ in (23b) includes the integration chain of $\mathbf{r}$ and θ from $\mathbf{u}$, namely

$$\frac{d}{dt}\begin{bmatrix} \mathbf{r}^T & \dot{\mathbf{r}}^T & \ddot{\mathbf{r}}^T & \theta & \dot{\theta} & \ddot{\theta} \end{bmatrix}^T = \begin{bmatrix} \dot{\mathbf{r}}^T & \ddot{\mathbf{r}}^T & \mathbf{u}_r^T & \dot{\theta} & \ddot{\theta} & u_\theta \end{bmatrix}^T, \tag{24}$$

as well as the sloshing dynamics in the containers as in (20b) and (20c). The passage through n_v way-volumes is imposed in equation (23h). Each way-volume is modeled as a sphere of radius δ centered at $\mathbf{r}_j$, and t_j denotes the time of passage through the j-th sphere, with $t_j \in (0, t_{end})$. Condition (23i) ensures

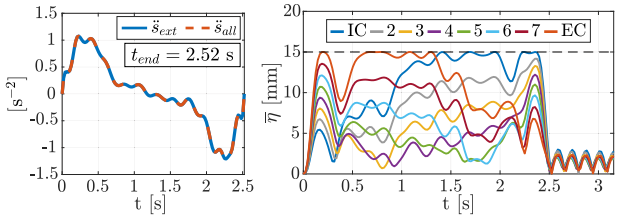

(a) Trends of $\ddot{s}$. (b) Sloshing heights of all containers.

Fig. 3. Influence of the number of containers.

(a) Robot and tray. (b) GoPro setup.

Fig. 4. Experimental setups.

TABLE II
OPTIMIZATION PARAMETERS

$k = 10^{-2}[\text{s}^6]$; $k_r = 10^{-3}[\text{s}^6/\text{m}^2]$; $k_\theta = 10^{-5}[\text{s}^6/\text{rad}^2]$; $k_{cond} = 0.03$
$u_{max} = 70[\text{s}^{-3}]$; $\mathbf{u}_{r,max} = 250[\text{m/s}^3]$; $u_{\theta,max} = 450[\text{rad/s}^3]$
$\mathbf{r}_{min} = [-\ \ -\ \ 0]^T[\text{m}]$; $\mathbf{r}_{max} = [-\ \ -\ \ 1][\text{m}]$
$\mathbf{q}_{min} = [-2.9\ \ -1.5\ \ -3.0\ \ -3.7\ \ -2.4\ \ -47.1]^T[\text{rad}]$
$\mathbf{q}_{max} = [2.9\ \ 2.7\ \ 0.0\ \ 3.7\ \ 2.4\ \ 47.1]^T[\text{rad}]$
$\dot{\mathbf{q}}_{max} = [2.4\ \ 2.8\ \ 3.0\ \ 7.9\ \ 6.5\ \ 9.6]^T[\text{rad/s}]$

that the computed path does not assume forbidden positions: this constraint is useful for collision-avoidance purposes, and it can be tailored to the specific case at hand. Condition (23j) guarantees that, throughout the motion, the position of each robot joint remains within permissible limits, thus ensuring that the trajectory stays within the robot workspace. Given $\mathbf{r}$ and θ, the optimizer determines the EE pose, and, by solving the robot inverse kinematics, determines the joint variables $\mathbf{q} \in \mathbb{R}^6$, which must satisfy constraint (23j). Constraint (23l) ensures a singularity-free optimal path (the inverse of the 2-norm condition number $\kappa(\mathbf{J})$ is used here, but any other equivalent criterion may also be used [20]). Regarding the remaining conditions of (23), the same considerations made in Section III-A apply.

C. Simplified Procedure for Identical Containers

Although the optimization algorithms presented in Sections III-A and III-B can handle sloshing-height constraints for any number of containers, even with different liquid height-to-radius ratios, they can be implemented more efficiently when all containers are identical and are filled with the same amount of liquid, which is the most common industrial scenario. In this case, the algorithms in (19) and (23) can be run by enforcing sloshing-height constraints only for the outermost containers (e.g., IC and EC in Fig. 2). This choice is supported by a large set of simulations, which have shown that constraining only these sloshing heights is sufficient, in most cases, to ensure compliance with the sloshing limits of all containers. This is justified by the fact that, for typical pick-and-place trajectories, the two outermost containers are subjected to the largest accelerations. This consideration allows the optimization algorithm to be independent of the total number of containers, thus ensuring high application flexibility and limited computation times even in the presence of many containers. An example that supports this observation is shown in Fig. 3(a), which illustrates the optimized trends of $\ddot{s}$ obtained by constraining only the 2 outer containers ($\ddot{s}_{ext}$) and by constraining all the 8 containers ($\ddot{s}_{all}$). It can be observed that the two trends are the same, thus representing the same solution to the optimization problem. Furthermore, by analyzing the computation times ($t_{comp,ext} = 85.1$ s, $t_{comp,all} = 471.4$ s), it is evident that constraining only the outermost containers leads to a significant benefit. The results shown in Fig. 3 refer to motion 1 A, which will be described in detail in Section IV-A. The sloshing-height trends of the 8 containers, resulting from the motion law in Fig. 3(a), are reported in Fig. 3(b), where it can be seen that each trend remains within the limit $\overline{\eta}_{lim} = 15$ mm. The labels 2 to 7 in Fig. 3(b) denote the intermediate containers.

Once an optimal trajectory has been obtained using the simplified procedure, a final simulation can be performed to verify that the sloshing heights of all containers remain below the assigned threshold; if this verification fails, the full optimization can then be run.

IV. EXPERIMENTAL VALIDATION

Experiments are conducted with 8 cylindrical containers arranged in a single row, with a center-to-center spacing of 90 mm. Since the dominant geometric parameter affecting the liquid dynamics is the ratio h/R, the container radius is kept constant at $R = 35$ mm, while three static liquid heights are tested: $h = 20$ mm, 30 mm, and 40 mm. For each case, the sloshing limit is set to $\overline{\eta}_{lim} = 15$ mm, while for $h = 40$ mm a limit of $\overline{\eta}_{lim} = 25$ mm is also tested. In Sections IV-A and IV-B, all containers are identical and the simplified optimization procedure described in Section III-C is used, whereas Section IV-C addresses the case of containers with different height-to-radius ratios, for which the full optimization is performed.

The robot chosen for trajectory execution is a 6-DOF *Comau SMART-SiX* (Fig. 4(a)). The liquid behavior during motions is recorded using two *GoPro Hero8* cameras attached to the tray, as shown in Fig. 4(b): the experimental sloshing height is extracted from the recorded videos. The optimization parameters used in (19) and (23) are summarized in Table II. The data sets of all motions described in this section are available at [21].

A. Experiments With Assigned-Path Trajectory Planning

Although numerous trajectories were tested for validation, only two are presented here for brevity:

- 1A: a standard semicircular pick-and-place path, represented by the blue curve in Fig. 5(a), with a total rotation of 2π (the tray rotation can be appreciated by noting the GoPro position circled in red);
- 2A: a complex pick-and-place path, represented by the blue curve in Fig. 5(b), with a total rotation of π.

Fig. 6(a)–(b) show the results for motion 1 A, and Fig. 7(a)–(b) for motion 2 A, with $h = 40$ mm and $\overline{\eta}_{lim} = 15$ mm. In particular, the graphs show the sloshing-height trends for containers IC (blue lines) and EC (red lines), obtained using the optimized motion law and a non-optimized one (a standard modified trapezoidal profile of $\ddot{s}$) with the same duration (for 1 A) and with a

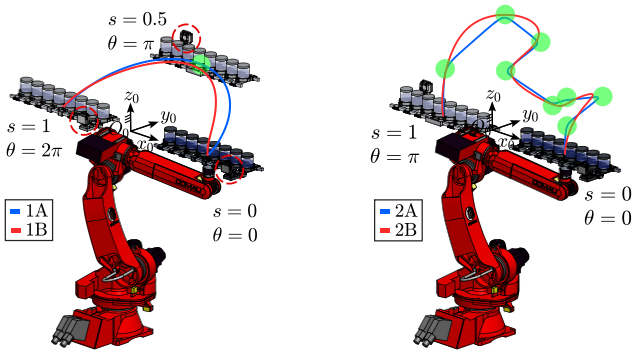

(a) Motions 1A and 1B. (b) Motions 2A and 2B.

Fig. 5. Experimental motions.

TABLE III
VALUES OF t_{end}, γ_{model}, AND γ_{opt} FOR ALL EXPERIMENTAL TESTS. PARAMETERS h AND $\overline{\eta}_{lim}$ ARE EXPRESSED IN MILLIMETERS

h	$\overline{\eta}_{lim}$			1A	1B	2A	2B		1A	2A
40	15	IC	t_{end}	2.25s	2.20s	4.29s	3.86s			
			γ_{model}	9.1%	25.3%	−23.0%	26.8%	γ_{opt}	52.8%	64.0%
		EC		11.6%	16.9%	12.1%	23.6%		54.1%	67.2%
40	25	IC	t_{end}	2.10s	1.82s	3.78s	3.80s			
			γ_{model}	1.8%	14.6%	−18.5%	15.4%	γ_{opt}	53.5%	18.4%
		EC		10.7%	9.5%	−23.6%	9.7%		47.0%	26.7%
30	15	IC	t_{end}	2.53s	2.20s	4.34s	3.87s			
			γ_{model}	18.0%	16.7%	4.6%	9.1%	γ_{opt}	55.2%	71.8%
		EC		0.3%	−0.4%	1.8%	6.1%		49.4%	72.1%
20	15	IC	t_{end}	2.58s	2.21s	4.49s	3.89s			
			γ_{model}	16.9%	13.7%	−7.2%	11.6%	γ_{opt}	49.7%	77.2%
		EC		−3.0%	−3.4%	−1.2%	4.4%		43.6%	73.3%

longer duration (for 2 A). The comparison between the modeled (continuous line) and experimental (dashed line) sloshing-height trends shows the effectiveness of the model in Section II in predicting the sloshing height, and it is quantitatively assessed through the index:

$$\gamma_{model} = 100\frac{\int_0^{1.25t_{end}} \left(\overline{\eta}_{model}(t) - \overline{\eta}_{exp}(t)\right) dt}{\int_0^{1.25t_{end}} \overline{\eta}_{model}(t) dt}, \qquad (25)$$

where the upper integration limit is set at $1.25t_{\text{end}}$ to also account for residual oscillations. Table III reports the ratios γ_{model} for all optimized motions described in this and the next subsection.

The benefit of using optimized motion laws is quantitatively evaluated through the index:

$$\gamma_{opt} = 100\frac{\overline{\eta}_{max,Nopt} - \overline{\eta}_{max,Opt}}{\overline{\eta}_{max,Nopt}}, \qquad (26)$$

where subscripts Opt and Nopt denote, respectively, the optimized and non-optimized experimental trends. The ratio γ_{opt} is also reported in Table III.

For the cases represented in Figs. 6(a) and 7(a), it can be seen that the sloshing height only slightly exceeds the imposed limit of $\overline{\eta}_{lim} = 15$ mm at certain time instants in motion 1 A, whereas the exceeding of the threshold, as well as the residual oscillations at the end of the motion, are more evident in motion 2 A. This is due to the fact that the sharp turns in the path of motion 2 A induce strong nonlinearities in the liquid motion, which the MSD model is unable to accurately capture. It is worth highlighting that motion 2 A has been used as an extreme case, presenting a highly challenging scenario for the optimizer, but it does not represent a realistic industrial pick-and-place motion. Despite this, the optimizer still delivers suitable solutions compared to non-optimized cases.

For completeness, some frames from the GoPro videos (from which the experimental sloshing-height trends have been extracted) are reported in Fig. 8. Specifically, Fig. 8(a) shows the EC at $t = 1.4$ s during motion 1 A with the optimized motion law, whereas Fig. 8(b) displays the EC at the same time instant during motion 1 A with the non-optimized motion law. In both frames, the sloshing peak is indicated with a red circle, and the dashed black curve denotes the imposed sloshing limit. The comparison between the two frames clearly shows the advantage in employing the optimized motion law. This effect is even more pronounced when considering motion 2 A. Fig. 8(c)–(d) show the maximum liquid peaks of the EC during motion 2 A with optimized and non-optimized motion laws, respectively. It can be seen that, in the non-optimized motion, even though the trajectory is significantly slower (6 s instead of 4.29 s), the liquid would have overflowed if the container had not been closed by the lid. This frame explains why, in Fig. 7(b), after the peak at $\overline{\eta} = 60$ mm (the height of the container lid), the experimental trends diverge from the simulated ones: this inconsistency is due to the impact with the lid, which drastically changes the liquid dynamics.

B. Experiments With Point-to-Point Trajectory Planning

This section highlights the advantages of point-to-point optimizations over those with an assigned path. One and eight spherical way-volumes, each with a radius of $\delta = 50$ mm, are defined along paths 1 A and 2 A, respectively, and are highlighted in green in Fig. 5(a) and (b). The optimized paths, denoted 1B and 2B, are shown in red in the same figures. Figs. 6(c) and 7(c) illustrate the time evolution of sloshing heights, both in simulation and in experiments, for motions 1 B and 2 B, corresponding to the case $h = 40$ mm and $\overline{\eta}_{lim} = 15$ mm. Compared to motion 2 A, the optimized path 2 B features smoother and wider curves; as a result, the nonlinear regimes that previously caused the sloshing height to exceed $\overline{\eta}_{lim}$ no longer occur. This can be verified in Fig. 7(c), which also shows reduced residual oscillations at the motion end.

The index γ_{model} reported in Table III also confirms the improvement. In particular, for trajectory 2 A (the most critical one), the model often underestimates the sloshing height (when γ_{model} takes negative values), resulting in higher experimental values and, thus, a greater risk of exceeding the imposed threshold. In contrast, for trajectories 2 B, γ_{model} is always positive, showing that the model overestimates the sloshing height, thus ensuring better compliance with the limit.

The improvement of trajectory 1 B with respect to 1 A is less pronounced, as the two motions follow similar paths. Nevertheless, the fact that γ_{model} is positive for both 1 A and 1 B in most cases confirms that the experimental sloshing height remains below the imposed limit.

Finally, comparing the values in Table III shows that the point-to-point strategy yields shorter motion durations. By allowing the path to vary, the optimizer faces fewer constraints and is therefore able to find better solutions. Indeed, the gentler curves

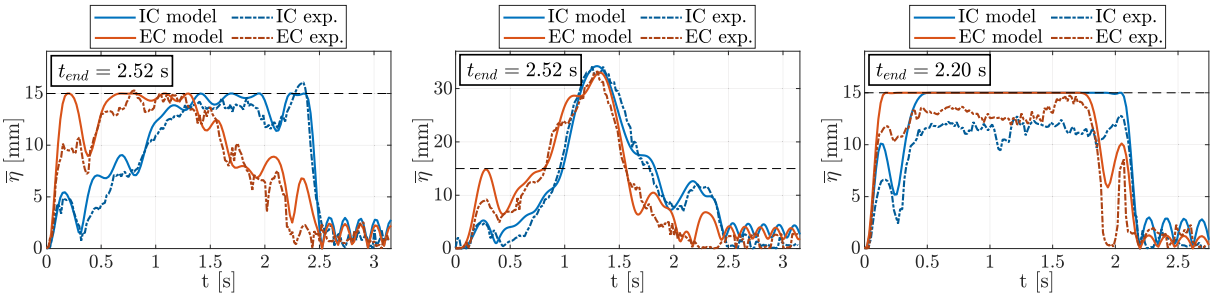

(a) 1A: optimized motion law, assigned path. (b) 1A: non-optimized motion law, assigned path. (c) 1B: optimized motion law, optimized path.

Fig. 6. Sloshing-height trends for motion 1, with $h = 40$ mm and $\overline{\eta}_{lim} = 15$ mm.

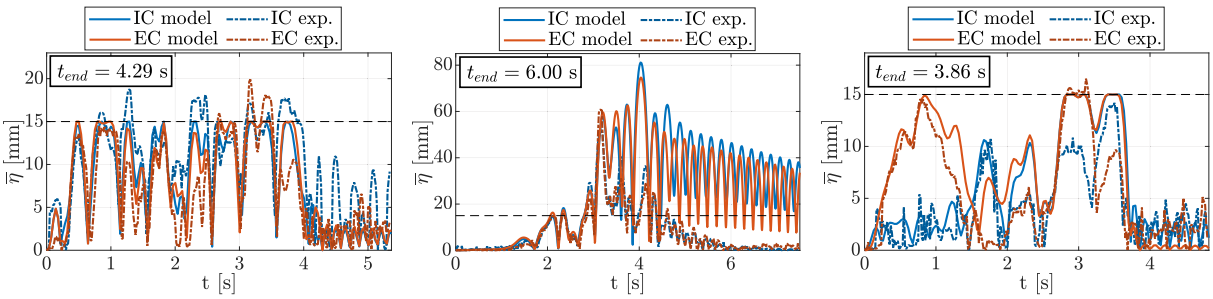

(a) 2A: optimized motion law, assigned path. (b) 2A: non-optimized motion law, assigned path. (c) 2B: optimized motion law, optimized path.

Fig. 7. Sloshing-height trends for motion 2, with $h = 40$ mm and $\overline{\eta}_{lim} = 15$ mm.

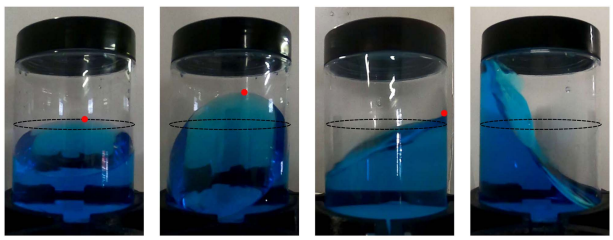

(a) 1A Opt. (b) 1A Nopt. (c) 2A Opt. (d) 2A Nopt.

Fig. 8. Container instant frames during motions.

of the optimized path enable faster traversal, since the larger curvature radii produce lower centripetal accelerations on the containers, thereby decreasing the liquid excitation.

C. Experiments in Generic Case

The proposed algorithms are capable of handling fully generic container configurations. To demonstrate this feature, using the experimental setup of Sections IV-A and IV-B, a scenario with eight containers and different filling heights ($h_{IC} = h_{EC} = 40$ mm, $h_2 = h_7 = 30$ mm, $h_3 = h_4 = h_5 = h_6 = 20$ mm) was considered, and the corresponding time-optimal trajectory for motion 2 A was computed considering $\overline{\eta}_{lim} = 15$ mm. Since it is not possible to determine *a priori* which containers exhibit the largest liquid oscillation, the sloshing-height constraint is imposed on all containers. The obtained trajectory, with a duration of $t_{end} = 4.44$ s was tested, and the corresponding experiment showed consistency with the simulation results, as confirmed by the values of γ_{model} and $\overline{\eta}_{max,exp}$ in Table IV. The dataset [21] also includes the results for motion 2 B.

TABLE IV
VALUES OF γ_{model} AND $\overline{\eta}_{max,exp}$ FOR THE GENERIC CASE

Container	IC	2	3	4	5	6	7	EC
γ_{model} [%]	6.1	6.1	-0.8	0.8	3.6	3.5	7.3	-2.1
$\overline{\eta}_{max,exp}$ [mm]	13.9	14.5	16.0	17.2	15.8	15.7	16.8	20.8

D. Computational Details

The computation of the sloshing-height trend along a single trajectory, such as those reported in Section IV, requires approximately 1 s, using a non-optimized MATLAB implementation on a PC equipped with an Intel Core i7 (8th generation) processor, 16 GB of RAM, and Intel UHD Graphics 620. The CasADi implementation of the optimization algorithms (19) and (23) requires approximately 85 s, 307 s, 97 s and 149 s, to compute the optimized trajectories in Figs. 6(a), 7(a), 6(c) and 7(c), respectively, with a variability of approximately 2% across repeated runs under identical conditions. The nonlinear programming (NLP) problem is solved with the Interior Point Optimizer (IPOPT). The time horizon is discretized into 151 sub-intervals, providing sufficient resolution to satisfy constraints both at the nodes and in between, without significantly increasing computational cost. A multiple-shooting scheme with fourth-order Runge–Kutta (RK4) integration is employed. The solver is configured with a maximum of 3000 iterations, and termination criteria require the NLP error, constraint violation, and dual infeasibility to fall below 10^{-8}.

V. CONCLUSION

This paper studied the time-optimal planning of anti-sloshing SCARA-type trajectories for the transport of multiple cylindrical

containers filled with liquid. First, a computationally-efficient sloshing-height estimation model suitable for 4D SCARA motions was presented. Then, two families of constrained optimizations were developed. In the first one, optimal motion laws were determined to follow assigned paths. In the second one, both the motion law and the path were optimized, with the latter constrained only to pass through assigned way-volumes. The proposed approach can handle any number of containers, even with different liquid height-to-radius ratios. When all containers are identical and filled with the same amount of liquid, a simplified version can be used that is independent of the number of containers, as it enforces sloshing-height constraints only for the outermost ones, thereby minimizing computational effort.

The optimized trajectories were validated through an extensive experimental campaign, consistently demonstrating superior performance compared to non-optimized trajectories. Among the two strategies, the point-to-point approach (where the path is optimized together with the motion law) proved to be the most effective, as it enabled shorter motion durations and ensured more accurate compliance with the sloshing-height limits, even in the presence of highly complex dynamical motions.

In the future, the proposed approach will be extended to so-called waiter motions (where the containers are not anchored to the tray but simply placed on it) and to full 6D motions, thus enabling tilting compensation.

REFERENCES

[1] J. Feddema, C. Dohrmann, G. Parker, R. Robinett, V. Romero, and D. Schmitt, "Control for slosh-free motion of an open container," *IEEE Control Syst. Mag.*, vol. 17, 1, pp. 29–36, Feb. 1997, doi: 10.1109/37.569711.

[2] L. Biagiotti, C. Melchiorri, and L. Moriello, "Optimal trajectories for vibration reduction based on exponential filters," *IEEE Trans. Control Syst. Technol.*, vol. 24, 2, pp. 609–622, Mar. 2016, doi: 10.1109/TCST.2015.2460693.

[3] N. C. Singer and W. P. Seering, "Preshaping command inputs to reduce system vibration," *ASME J. Dyn. Systems, Meas., Control*, vol. 112, no. 1, pp. 76–82, 1990, doi: 10.1115/1.2894142.

[4] L. Guagliumi, A. Berti, E. Monti, and M. Carricato, "Anti-sloshing trajectories for high-acceleration motions in automatic machines," *ASME J. Dyn. Syst., Meas., Control*, vol. 144, no. 7, pp. 1–14, 2022, doi: 10.1115/1.4054224.

[5] L. Biagiotti, D. Chiaravalli, L. Moriello, and C. Melchiorri, "A plug-in feed-forward control for sloshing suppression in robotic teleoperation tasks," in *Proc. IEEE/RSJ Int. Conf. Intel. Robots Syst.*, Madrid, Spain, 2018, pp. 5855–5860, doi: 10.1109/IROS.2018.8593962.

[6] J. Reinhold, M. Amersdorfer, and T. Meurer, "A dynamic optimization approach for sloshing free transport of liquid filled containers using an industrial robot," in *Proc. IEEE/RSJ Int. Conf. Intel. Robots Syst.*, Macau, China, 2019, pp. 2336–2341, doi: 10.1109/IROS40897.2019.8968144.

[7] R. Muchacho, R. Laha, L. Figueredo, and S. Haddadin, "A solution to slosh-free robot trajectory optimization," in *Proc. IEEE/RSJ Int. Conf. Intel. Robots Syst.*, Kyoto, Japan, 2022, pp. 223–230, doi: 10.1109/IROS47612.2022.9981173.

[8] F. Brasina, L. Guagliumi, R. Di Leva, and M. Carricato, "Anti-sloshing motion laws for one-dimensional piecewise trajectories," in *New Trends Mechanism Mach. Sci. - Proc. EuCoMeS 2024, Mechanisms Mach. Sci.*, Padua, Italy, Springer, eds. G. Rosati, A. Gasparetto, and M. Ceccarelli, 2024, vol. 165, pp. 153–162, doi: 10.1007/978-3-031-67295-8_18.

[9] W. Aribowo, T. Yamashita, and K. Terashima, "Integrated trajectory planning and sloshing suppression for three-dimensional motion of liquid container transfer robot arm," *J. Robot.*, vol. 2015, pp. 1–15, 2015, doi: 10.1155/2015/279460.

[10] R. Di Leva, M. Carricato, H. Gattringer, and A. Muller, "Time-optimal trajectory planning for anti-sloshing 2-Dimensional motions of an industrial robot," in *Proc. 20th Int. Conf. Adv. Robot.*, Ljubljana, Slovenia, 2021, pp. 32–37, doi: 10.1109/icar53236.2021.9659383.

[11] K. Zauner, H. Gattringer, and A. Müller, "Time-optimal transport of loosely placed liquid filled cups along prescribed paths," in *Proc. Adv. Serv. Ind. Robot. - RAAD 2024, Mechanisms Mach. Sci.*, Cluj-Napoca, Romania, Springer, Eds. D. Pisla, G. Carbone, D. Condurache, and C. Vaida, 2024, vol. 157, pp. 411–419, doi: 10.1007/978-3-031-59257-7_41.

[12] H. Gattringer, A. Müller, S. Weitzhofer, and M. Schörgenhumer, "Point to point time optimal handling of unmounted rigid objects and liquid-filled containers," *Mechanism Mach. Theory*, vol. 184, 2023, Art. no. 105286, doi: 10.1016/j.mechmachtheory.2023.105286.

[13] J. Andersson, J. Gillis, G. Horn, J. Rawlings, and M. Diehl, "CasADi: A software framework for nonlinear optimization and optimal control," *Math. Program. Comput.*, vol. 11, no. 1, pp. 1–36, 2019, doi: 10.1007/s12532-018-0139-4.

[14] R. A. Ibrahim, *Liquid Sloshing Dynamics: Theory and Applications*. Cambridge U.K.: Cambridge Univ. Press, 2005, doi: 10.1017/CBO9780511536656.

[15] H. Bauer, "Nonlinear mechanical model for the description of propellant sloshing," *AIAA J.*, vol. 4, pp. 1662–1668, 1966, doi: 10.2514/3.3752.

[16] L. Guagliumi, A. Berti, E. Monti, and M. Carricato, "A simple model-based method for sloshing estimation in liquid transfer in automatic machines," *IEEE Access*, vol. 9, pp. 129347–129357, 2021, doi: 10.1109/ACCESS.2021.3113956.

[17] R. Di Leva, M. Carricato, H. Gattringer, and A. Müller, "Sloshing dynamics estimation for liquid-filled containers performing 3-Dimensional motions: Modeling and experimental validation," *Multibody Syst. Dyn.*, vol. 56, no. 2, pp. 153–171, 2022, doi: 10.1007/s11044-022-09841-0.

[18] H. Bauer, "Tables of Zeros of Cross Product Bessel Functions," *Math. Comput.*, vol. 18, no. 85, pp. 128–135, 1964, doi: 10.1090/S0025-5718-1964-0158105-5.

[19] R. Di Leva, S. Soprani, G. Palli, L. Biagiotti, and M. Carricato, "Sloshing-height estimation for liquid-filled containers under four-dimensional motions including spatial translation and rotation about a fixed direction: Modeling and experimental validation," submitted, 2025.

[20] J. P. Merlet, "Jacobian, manipulability, condition number, and accuracy of parallel robots," *J. Mech. Des.*, vol. 128, no. 1, pp. 199–206, 2005, doi: 10.1115/1.2121740.

[21] A. Ferrari, R. Di Leva, S. Soprani, L. Biagiotti, G. Palli, and M. Carricato, "Time-optimal anti-sloshing trajectory planning for multiple liquid-filled containers subject to SCARA motion," [Data set] Zenodo, 2025, doi: 10.5281/zenodo.16309246.